Development of the new long trace profilometer at LCLS for bendable x-ray mirror metrology

M. L. Ng, J. Nicolas, D. Spiga, C. L. Hardin, D. S. Morton, et al.

M. L. Ng, J. Nicolas, D. Spiga, C. L. Hardin, D. S. Morton, D. Cocco, "Development of the new long trace profilometer at LCLS for bendable x-ray mirror metrology," Proc. SPIE 10761, Adaptive X-Ray Optics V, 1076106 (17 October 2018); doi: 10.1117/12.2323293

SPIE.

Event: SPIE Optical Engineering + Applications, 2018, San Diego, California, United States

Development of the new Long Trace Profilometer at LCLS for bendable X-ray mirror metrology

M. L. Ng[1], J. Nicolas[2], D. Spiga[*1,3], C. L. Hardin[1], D. S. Morton[1], D. Cocco[1]

[1]SLAC National Accelerator Laboratory, 2575 Sand Hill Road, 94025 Menlo Park (USA)
[2]ALBA Synchrotron Light Source, Carrer de la Llum 2-26, 08290 Cerdanyola del Vallés, Spain
[3]INAF – Brera Astronomical Observatory, Via Bianchi 46, 23807, Merate (Italy)

ABSTRACT

The Linac Coherent Light Source (LCLS) is undergoing an upgrade to a double source setup to provide eight experimental hutches (five existing and three new) with either high-repetition or high-intensity pulses and highly coherent X-ray beams. The photon transportation and distribution to each hutch relies on, among other elements, bendable mirrors. Given the coherence of the LCLS source, and to avoid introducing wavefront distortions beyond workable limits, the mirrors need to have extremely smooth surfaces, with a figure compliant with the nominal profile (usually elliptical). The effectiveness and the accuracy of the bending system and of the actuators over the entire length of the mirror (up to 1.2 m) need to be assessed by an appropriate metrology system. Long Trace Profilometry (LTP) is a suitable technique to characterize a slightly-curved surface mirror profile with very high sensitivity, provided that the optomechanical system implementation enables sensitivity and accuracy values compatible with the mentioned surface quality requirements. In this paper, we show the status and performance of the LTP under development at LCLS. The LTP essentially consists of an advanced optical head that endows a laser beam with sharp interferential features to increase its resolution and detects the optical lever of the beam reflected by the sample, plus a high-precision gantry system (Q-Sys) for accurate scanning of the mirror under test, under impact of its bending mechanics and cooling system. The measured results are compared to the simulated performance of the LTP, and we show the way of the oncoming improvement of the instrument.

Keywords: Long Trace Profilometer, LCLS, bendable mirrors, metrology, slope detection, pentaprism

1. INTRODUCTION

The Linac Coherent Light Source (LCLS)[1] at SLAC national accelerator laboratory is being upgraded to improve its optical performances. A major reconstruction of the entire facility, which will ultimately endow it with an additional accelerator (LCLS-II), is currently in progress. The new accelerator will be equipped with superconducting cavities in order to bring the pulse repetition rate to about 1 MHz, vs. the 120 Hz of the currently operating source that employs a copper accelerator. LCLS-II will be, in fact, the first X-ray free-electron laser able to supply a uniformly-spaced train of pulses with programmable repetition rate.

Five existing beamlines will be maintained, plus three additional ones (TMO, TXI, and NEH 2.2) that will be located in the near experimental hutch (NEH).[2] The beam delivery to each beamline will be ensured by a front-end enclosure (FEE) committed to perform the photon flux delivery without compromising its spatial and temporal coherence. For this reason, the optical elements for moderating the beam shall exhibit excellent profile accuracy (close to 1 nm rms over the entire mirror length) and surface finishing (on the order of 0.3 nm rms or less). Any surface defect would, in fact, leave an imprint in the wavefront propagation that will ultimately affect the coherence preservation and the final focusing performances in the beamlines, which should be close to the diffraction limit. This clearly sets stringent limits on the tolerances for the mirror fabrication.

In this all, metrology plays a primary role. Passive mirrors and actively bent mirrors need to be characterized to very high precision for making them compliant with the scientific goals that are relevant to each beamline. Not surprisingly, a relevant effort is being deployed at LCLS aiming at improving the metrology equipment and the testing environment. A completely new building (with operation expected in fall 2018) will house the

*e-mail: spigasan@slac.stanford.edu, phone: +1-650-924-3070

Adaptive X-Ray Optics V, edited by Daniele Spiga, Hidekazu Mimura, Proc. of SPIE Vol. 10761, 1076106 · © 2018 SPIE · CCC code: 0277-786X/18/$18 · doi: 10.1117/12.2323293

metrological instrumentation and provide a vibration-free, thermally stable enclosure to ensure a repeatability level compatible with the accuracy levels mentioned above.

Metrological equipment can be of various kind, depending on the spatial periods that need to be characterized, the level of sensitivity, and the optic shape. For example, interferometers can reach extreme accuracies and precision values, but their dynamic range is usually limited unless they are equipped with wavefront adapters (e.g., computer-generated holograms) that match the testing wavefront to the nominal shape of the optic. Aiming to measure the profile of grazing-incidence mirrors over their entire length, an instrument with the optimal characteristics was developed since the early 80's:[3,4] the Long Trace Profilometer (LTP) is a versatile device for surface slope detection. In its essential design, an LTP casts a thin, collimated laser beam of the surface to be tested: the reflected beam is then imaged on a position-sensitive detector, from which the slope variation can be retrieved while the profile is scanned. The height profile is simply obtained by integration of the slope scan. This design allows the user to reconstruct a single profile at a time in the mirror's tangential plane; it also evolved towards a more sophisticate design, involving many laser beams operated in parallel[5] for the simultaneous detection of many parallel profiles.

In the early versions of the LTP (circa 1990), all the optical head was scanned over the mirror length; hence, the system was not only sensitive to the surface slope variations, but also to the oscillations of the optical head during the measurement. At that time, the problem was solved splitting the laser beam and sending one onto a fixed reference mirror: in this way, the optical head's weaving movement could be detected and subtracted from the measurement. However, it became clear in the 90's that the complication of the reference mirror could be removed by having a pentaprism scan the sample, keeping the optical head still.[6] A pentaprism has the remarkable property that the beam is always deflected by a right angle toward the surface to be tested, regardless of the angle the laser forms with the entrance face: therefore, small oscillations in the scanning stage have no effect on the recorded slope.

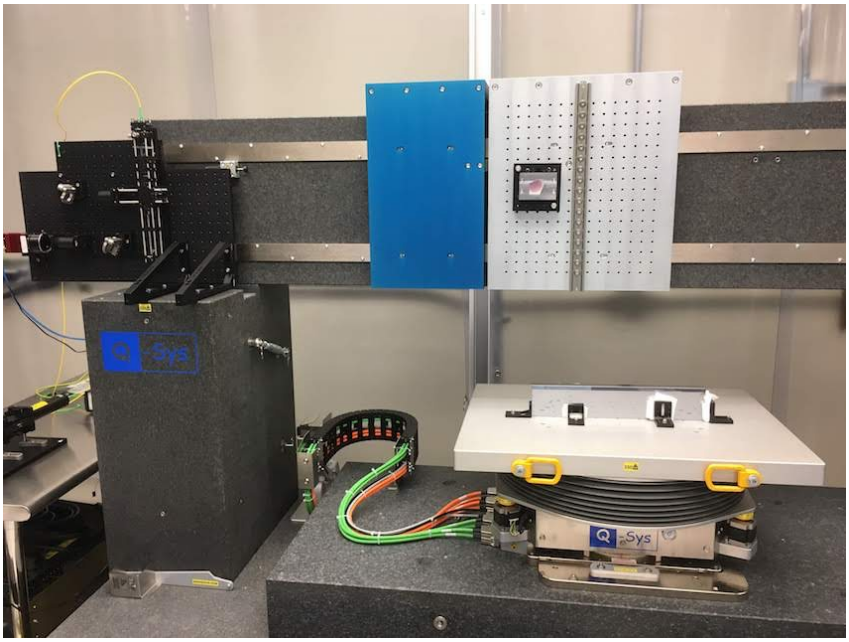

Figure 1. The new LTP in the LCLS labs. The fixed optical head (see detail in Fig. 4) is visible on the left side. The gantry system performs the scan of the pentaprism (on the central stage) over the mirror length. The mirror under test can be moved in the other five degrees of freedom by another granite stage and the tip-tilt-rotate table which the sample is mounted on.

A more advanced version of an LTP replaces the light source and the optical head with an autocollimator[7,8] to probes the sample surface. The beam is deviated to the surface by a pentaprism, and the angle between the incident and the reflected angle can be measured very precisely, if the varying distance to the sample is

known. The latest version of the LTP replaces all the optical system by a Shack-Hartmann optical head,[9,10] which directly sheds a light beam onto the sample and detects the reflected wavefront. The wavefront analysis then enables accurate metrology of the illuminated portion of the mirror, and a stitching algorithm joins all the exposures into a consistent mapping of the surface. Application of wavefront sensing techniques in X-rays is routinely operated for accurate metrology of Kirkpatrick-Baez[11] mirror systems at the DiProi beamline at the Fermi light source.[12]

In this paper, we describe the advancement status in the assembly of the novel LTP at LCLS (Sect. 2). The instrument is not installed yet in an optimal environment for metrology (i.e., thermally stable and isolated from vibrations/air turbulences); neither are the optical components optimized for a height detection accuracy of a few nanometers. While the system is expected to be moved to a dedicated clean room before the end of 2018, the current optical components need to be replaced with new ones with more demanding specifications. Section 3 describes the initial system calibration and the assessment of measurement errors. The subsequent step consists in ascertaining the fabrication tolerances of the optical parts that moderate/deviate the beam after the reflection on the sample mirror to be characterized, and that consequently introduce spurious slope changes during the sample scan. This might occur, for example, when short curvature radius mirrors are characterized and so the full slope detection range is explored. In Sect. 4, we reproduce the measured errors of the system from the manufacturing tolerances of the optical components currently in use, and show the improvement expected from the adoption of more advanced elements.

2. THE OPTICAL LAYOUT OF THE NEW LTP AT LCLS

2.1 The gantry system

The LTP that has been assembled at LCLS for characterizing the tangential profile of deformable mirrors is based on the scanning pentaprism concept. In order to ensure a precise and repeatable alignment and measurement of the mirrors, the metrology platform of the instrument (Fig. 1) is a gantry system in granite (mod. 298-01 by Q-Sys), equipped with motion controls and feedback via optical encoders, with a linear resolution < 30 nm. The optical head that generates, processes, and analyses the laser beam is fixed on the left side of the instrument. The scanning stage carries a pentaprism to scan the mirror length (the x-axis) and can also operate a stitching wavefront sensor in parallel to the pentaprism. The laser beam is reflected by the surface under test (SUT) according to the local surface slope, and bounced back via the pentaprism to the optical head, where the beam displacement is recorded by a CCD camera. The gantry system also enables the mirror stage translation along the sagittal direction (y-axis), adjustment in height (the z-axis), and tip-tilt-rotation movements via precision motors and accurate optical encoders. All the stages are mounted onto air bearings to ensure smooth and repeatable displacements.

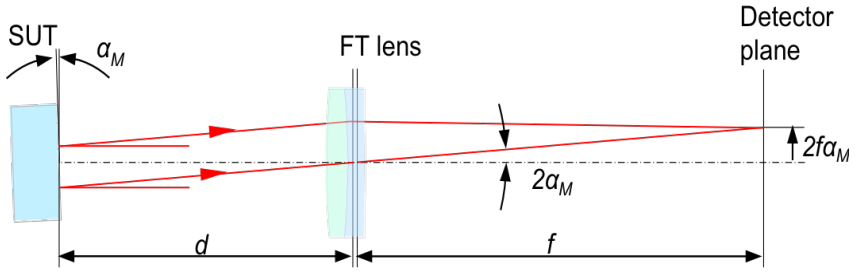

Figure 2. Geometry of the Fourier Transform lens. It is a lens system characterized by low distortion, i.e., high linearity in the conversion from the angular space (left) to the coordinate space (right). If the camera is placed in the lens focus, the lateral displacement is independent of the location where the beam crosses the lens.

As already mentioned, the adoption of a fixed optical head plus a scanning pentaprism removes the need of a reference mirror to subtract the carriage oscillations from data. This is exactly true, however, only if a the pentaprism has a shape within acceptable tolerances. In this setup, moreover, the SUT-to-CCD total distance, d, continuously changes during the scan. In order to completely de-couple the slope measurement from the laser range, a Fourier Transform lens (FTL) with diameter Φ_L is placed in the optical head (Fig. 2). The SUT-FTL

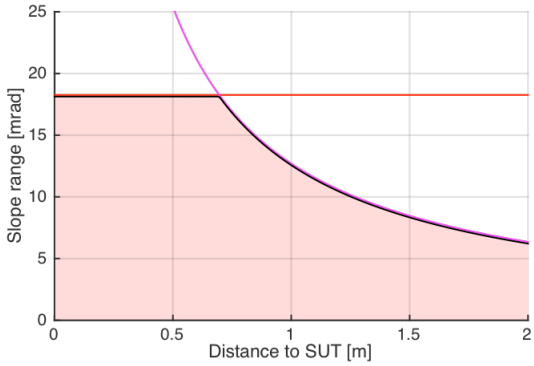

Figure 3. Explorable ranges of mirror slopes (colored area) as a function of the SUT-FTL distance. We have assumed a FTL with 1 inch diamter, a 500 mm focal length of the FTLs, and a 18.4 mm CCD camera.

optical range affects, indeed, the range of measurable slopes. This is more often determined by the CCD size, Y_c, and the FTL focal length f, as the maximum slope detected within the camera field is $\alpha_M = Y_c/4f$. On the other hand, if the lateral displacement $2\alpha_M d$ at the FTL aperture exceeds its radius $\Phi_L/2$, the beam is not imaged by the lens. The maximum detectable slope is therefore

$$\alpha_M = \pm \min\left(\frac{Y_c}{4f}, \frac{\Phi_L}{4d}\right), \tag{1}$$

and the measurable slope range, $2\alpha_M$, is displayed in Fig. 3 for $f = 500$ mm, $\Phi_L = 25.4$ mm, and $Y_c = 18.4$ mm. We note that for medium-to-large values of d, the measurement range is mostly limited by the diameter of the FTL. The current setup includes a 1"-diam. lens: in order to expand the measurement range, a re-furbished optical FTL with a 2" diameter will be procured.

2.2 The optical head

The optical head of the LTP in its current configuration[13] is shown in Fig.4. Following the laser path through it, we distinguish four sections ("branches") in the optical element sequence.

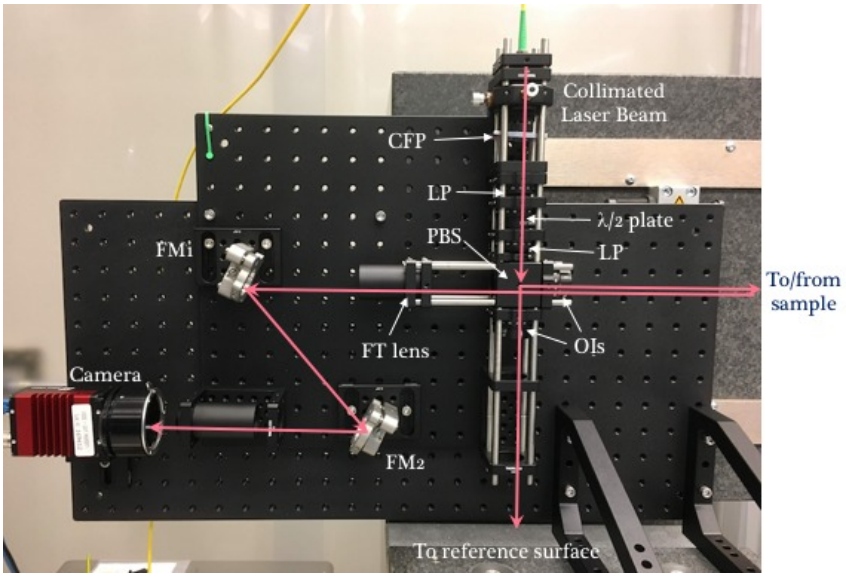

Figure 4. Picture of the LTP optical head. The laser path is shown when crossing the various optical components: CFP, central fringe plate; LP, linear polarizer; PBS, polarizing beam splitter; OI, optical insulator; FT, Fourier transform lens; FM, folding mirror.

1. Branch 1 (beam generator):

   - Laser source: a He-Ne laser, driving a 632.8 nm laser light to the LTP via an optical fiber. At the fiber exit, the beam is diverging and, owing to the fiber birefringence, elliptically polarized.
   - Collimating lens: an aspheric lens is placed after the beam for reducing its divergence to an acceptable level. The residual divergence is mainly caused by the self-diffraction of the Gaussian beam after the beam collimation by the lens. Long focal lengths entail a broader beam at the lens exit and a divergence decreasing in inverse proportion with the beam width. Three collimators were purchased with different focal lengths (5 mm, 8 mm, and 11 mm) for optimizing the beam collimation. The focal distance is adjustable within 1 mm travel range.
   - Central Fringe Plate (CFP): shortly after collimation, the beam crosses the junction between two thin glass foils, located side-to-side and forming a small angle, so to create a $\lambda/2$ delay in one half of the beam. This generates a dark fringe in the middle of the laser spot.[14] Locating the intensity minimum in the camera returns a much sharper measurement of the local slope than with other methods (e.g., based on the centroid location). A plate thickness of nearly 400 μm, assuming a 1.52 refractive index and a 3.04° angle between the two plates, was expected from simulations (Fig. 5A) to return an optimal fringe contrast. The CFP has been realized using Corning glass foils: after aligning carefully the laser and the plate, we could obtain a sharp fringe in the middle of the beam (Fig. 6B).

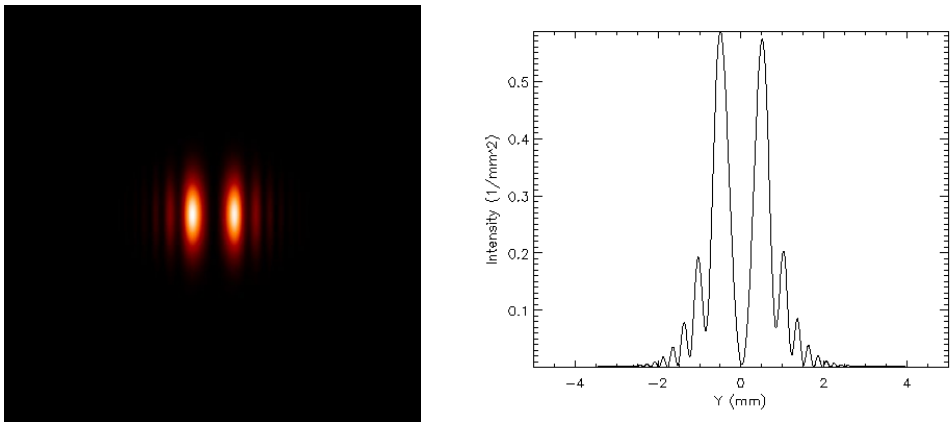

A) B)

Figure 5. A) Simulated laser intensity distribution after crossing the CFP. The thin glasses were 400 μm thick, forming a 3.2° mutual angle and a 0.35° angle with the incident beam. B) Central section along the x-axis. We notice the central sharp minimum. We have assumed a Gaussian beam with 0.5 mm rms. The image is 10 mm wide.

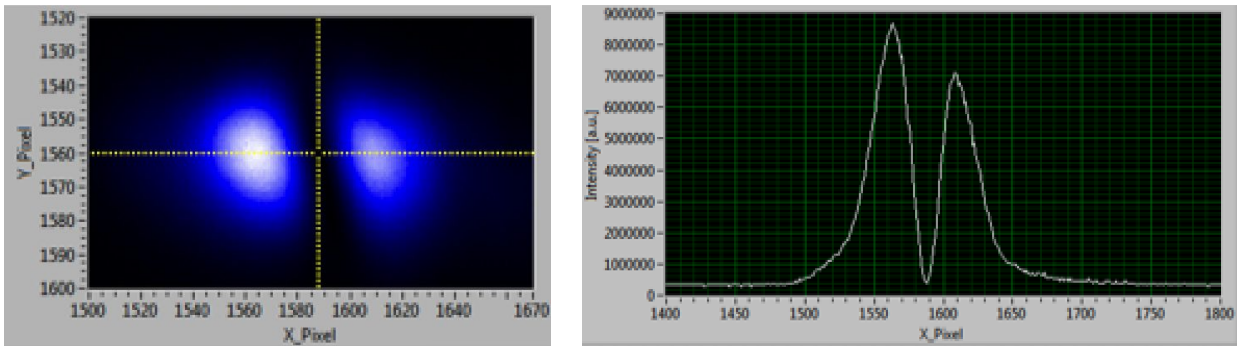

A) B)

Figure 6. A) The laser spot imaged in the CCD camera, and B) its median section. The minimum position is also affected by the CFP alignment, and its centering requires a careful tuning of the tip-tilt angles.

- Linear polarizer (LP) No. 1: polarizes the beam linearly, for subsequent moderation.
- Rotatable $\lambda/2$ plate: maintains the linear polarization state, changing the polarization plane.
- Linear polarizer (LP) No. 2: attenuates the beam intensity to convenient levels for alignment or measurement.

2. Branch 2 (to sample):

   - Polarizer Beam Splitter (PBS) cube: splits orthogonal polarizations into branch 2 and branch 3. Depending on the $\lambda/2$ plate orientation, the intensities of the beams toward the sample and the references can be adjusted to match the respective reflectivity values.
   - Optical insulator (OI) No. 1: a rotatable $\lambda/4$ plate that, after being crossed forth and back, prevents light from being deviated into branch 3, and so generate stray reflections.
   - Pentaprism (5P): deviates the beam to/from the sample by a right angle, regardless of tilt changes during the scan.
   - Sample under test (SUT): introduces into the beam the angular deviation to be measured. The beam reflected by the SUT re-enters in the pentaprism and is deviated to branch 4 via the OI No. 1 and the PBS.

3. Branch 3 (to reference):

   - Optical insulator (OI) No. 2: prevents light from being deviated into branch 2 and cause stray rays.
   - Reference mirror: when fixed to a platform separated from the optical head, it returns information about the vibration of the optical head. After reflection, the beam is sent to branch 4 via the OI No. 2 and the PBS.

4. Branch 4 (to the CCD camera):

   - Fourier Transform Lens (FTL): converts the angular deviation caused by the mirror under test (and the other optical components crossed/reflected by the beam between the sample and the FTL) into a spatial coordinate on the CCD.
   - Folding mirror No. 1 (FM1): folds the beam by nearly 135°, in order to fit the FTL-CCD distance to the focal length in a limited space.
   - Folding mirror No. 2 (FM2): folds the beam by nearly 135° to the camera.
   - CCD camera with 18.13 mm × 13.6 mm sensitive area and 5.5 μm pixel size. It records the beam position in the FTL focal plane. If the location of the beam central minimum is found via a best-fit routine, the displacement can be measured with great sensitivity (up to 0.03 times the pixel size,[5] i.e. ~ 0.2 μm in our case).

3. EXPERIMENTAL CALIBRATION

In this section, we determine the conversion factor between slope and CCD camera readout, and we measure the current deviations of the LTP from the ideal behavior. We denote the local slope of the SUT as m_0. The probing beam returns to the pentaprism with a $2m_0$ angular deviation and, if no spurious deflections are caused by the pentaprism, it impinges on the FTL after traveling a total distance d. Both m_0 and d change with the tangential coordinate, x, during the scan. The beam therefore crosses the FLT at a lateral distance $m_0 d$ from the optical axis. After the refraction in the FTL, the beam propagates via two bounces on the FMs over a distance D in air, until it is detected on the CCD array. Assuming the beam as paraxial and using the ABCD matrices notation, the coordinate-slope vector on the camera can be written as

$$\begin{pmatrix} y_c \\ m_c \end{pmatrix} = \begin{pmatrix} 1 & D \\ 0 & 1 \end{pmatrix} \begin{pmatrix} 1 & 0 \\ -1/f & 1 \end{pmatrix} \begin{pmatrix} 2m_0 d \\ 2m_0 \end{pmatrix}, \tag{2}$$

where the matrices express, from right to left, the beam deviation in the FTL and a free propagation through a distance D. We obtain

$$y_c = 2\left[D + \left(1 - \frac{D}{f}\right) d\right] m_0, \tag{3}$$

and the term in square brackets is the conversion factor between the doubled mirror slope and the y-coordinate on the camera. If the camera is exactly in the focus of the FTL, $D = f$, the beam position is made independent of d:

$$y_c = 2 f m_0. \tag{4}$$

In contrast, if the CCD is not precisely located in the focal plane of the lens, the conversion factor does depend on d, a clearly unwanted situation. The impact of the mismatch depends on the camera field covered while the SUT is scanned, i.e., on the m_0 range that is measured. Mirrors with small curvature radii exhibit more pronounced variations in the tangential slope, and the error increases in proportion. In order to find the best focus condition and so make Eq. 4 valid, we have performed an angular calibration of the LTP at five different values of d.

We have placed a flat, highly-polished silicon mirror on the tip-tilt-rotation stage (Fig. 1), and we have simulated a slope change tilting the stage at discrete x locations. We have explored the full measurement range of the LTP, initially probing the mirror near its center, corresponding to an initial FTL-SUT distance $d_0 =$ 1820 mm, in 0.01° steps. At this distance, the measurable slope range is approx. 5 mrad, in agreement with Fig. 3, and it is limited by the 1" diameter of the FTL (Fig. 4).

The longitudinal tilts measured by the accurate encoders in the gantry system have been compared with the displacements of the laser beams central minimum on the CCD. To check the repeatability caused by transient factors (air turbulence, vibrations, thermal fluctuations), each scan has been repeated a few times. The result for the central scan are shown in Fig. 7A.

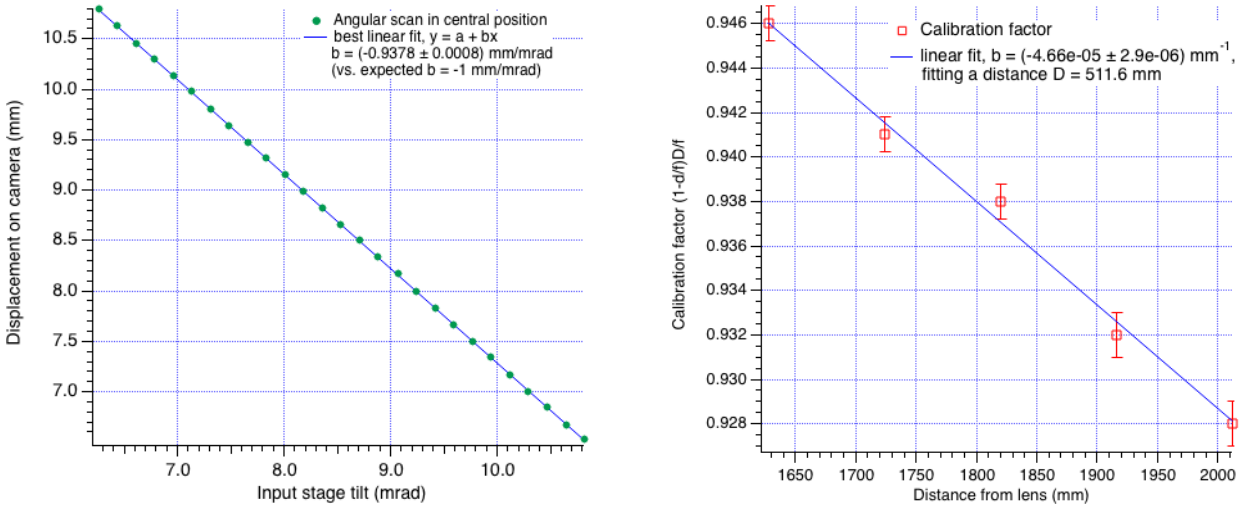

A) B)

Figure 7. Calibration run No. 1. A) Angular scan on central position, beam displacement on camera recorded vs. angular tilt imparted to rotation stage. The linear fit yields a slope coefficient that is significantly different from unity. B) The variation of the conversion factor with the distance from the FTL. The line slope allows us to infer the actual lens-camera distance and correct it.

As $f = (500 \pm 1)$ mm, in best focusing conditions the conversion factor would be 1000 mm/rad, i.e. 1 mm on the camera would correspond to 1 mrad. In a mrad-mm plot, the calibration line should therefore have slope coefficient 1. Figure 7A conversely shows that the calibration line differs significantly from 1 (the negative sign is just related to the orientation of the image in the camera), due to the misplacement of the camera with respect to the FTL focal plane. Repeating the calibration at different SUT locations, moreover, we find a significant

variation of the calibration factor on d (Fig. 7B). In agreement with Eq. 3, the dependence is linear. We point out that the variation with d was accurately measured by the encoders of the metrology platform, and the relative displacement has been sufficient to infer the slope of the line in Fig. 7B. The absolute distance d impacts only an additive constant in Eq. 3 and does not need to be determined. From the measured value of the slope coefficient $(1 - D/f)/f$ = -4.7 $\times 10^{-5}$ mm^{-1}, we can infer D = 511.6 mm, i.e. the camera is 11.6 mm extra-focal.

For the subsequent calibration test, we have approached the FTL to the CCD by approx. 11 mm and repeated the analysis. The five angular scans were taken at the same distances along the x-axis, and all the scans were repeated a few times to assess the measured error significance. We report in Fig. 8A the slope-displacement linear correlation for the scan in the central position. We have, this time, a slope much closer to the nominal value of 1 mm/mrad, confirming that the FTL position correction was performed in the correct direction. The same situation occurs at the other mirror locations, even if some variation in the conversion factor is still detectable. The dependence on d is much weaker this time, and the best linear fit is consistent with a FTL misplacement of just 1.5 mm (Fig. 8B).

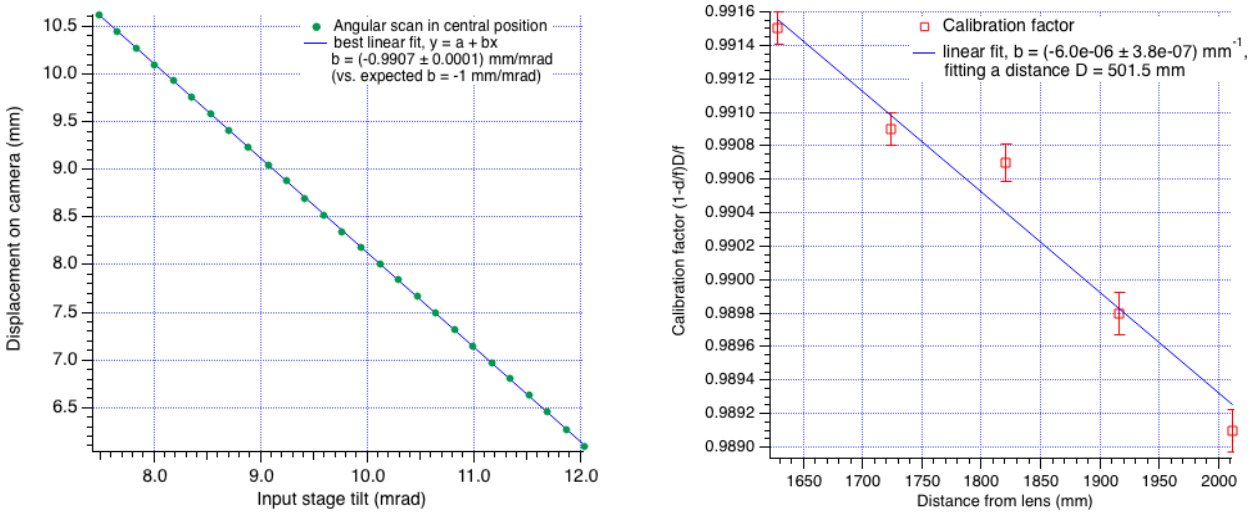

A) B)

Figure 8. Calibration run No. 2, after approaching the lens to the camera by ∼11 mm. A) Angular scan on central position, beam displacement on camera recorded vs. angular tilt imparted to rotation stage. The linear fit yields a slope coefficient much closer to unity. B) Variation of the conversion factor with the distance from the FTL. The variation is smaller than in Fig. 7, so we now derive a distance to best focus of just 1.5 mm.

In the current configuration, the deviation between the measured data and the best-fit line in Eq. 8A amounts to several microns (Fig. 9) with quite repeatable oscillations, much ampler than the measurement instabilities. Moreover, repeating the angular scan at different mirror locations nearly yields the same pattern within the measurement uncertainties. On this plate scale, these errors are equivalent to 20 μrad peak-to valley over a measured slope range of 4.5 mrad. While the error bars denote instability caused by the sub-optimal environment, the repeatable component of the oscillations can be ascribed to imperfections of the optical components. In the next section, we simulate the slope measurement errors from the current manufacturing tolerances, and we will see that they are consistent with the experimental result in Fig. 9.

4. PERFORMANCE SIMULATION

In this section, we model the measured errors in the angular scan of the LTP. Writing the simulation code, we have made the following assumptions:

- the beam coming from branch 1 of the optical head stands still, i.e., it maintains stable characteristics (divergence, brightness, size);

- the pentaprism scan direction is parallel to the beam;
- the beam is aligned parallel to the scan axis;
- the rotation stages are affected by a negligible error;
- the FT lens works in paraxial conditions.

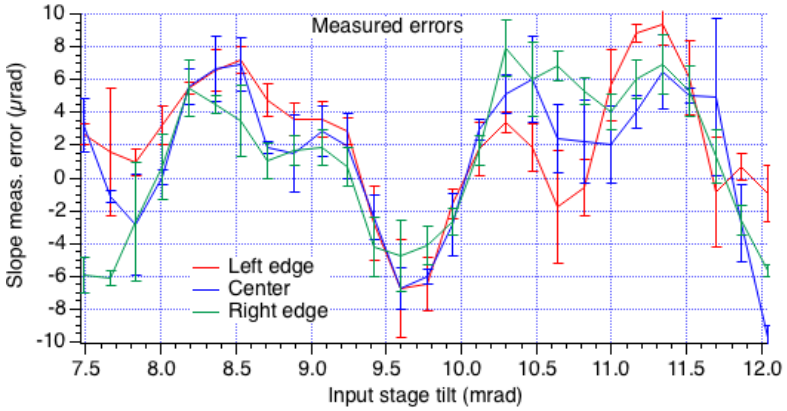

Figure 9. Some fit residuals from the calibration run No. 2, showing a several micron discrepancy from the linear dependence. Their patterns are consistent within the measurement repeatability, which suggests an insufficient quality of the optical elements.

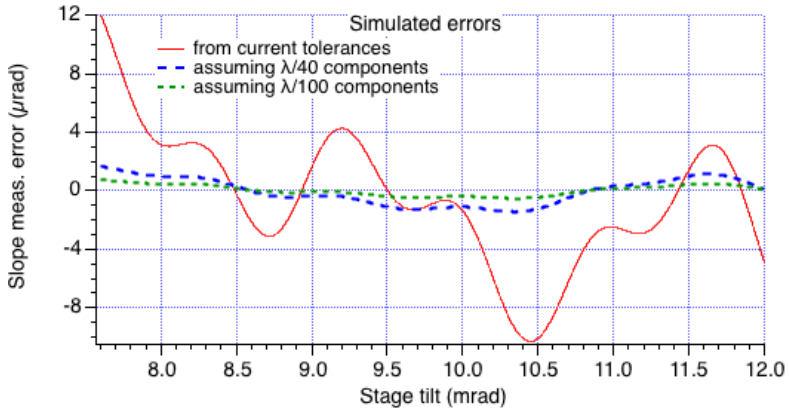

Figure 10. Solid line: slope measurement errors, simulated from the nominal manufacturing tolerances of the components in the branch 2 and 4 of the LTP (Fig. 4). We assumed a $\lambda/20$ 5P, a $\lambda/100$ OI, a $\lambda/10$ PBS, a $\lambda/4$ FTL, and FMs with a surface finishing of $\lambda/10$. The error signal qualitatively resembles the measured errors (Fig. 9, same axis ranges). Dashed lines: the same simulation assuming optical components with improved quality.

Based on these assumptions, we could simulate a scan of the slope measurement range (that, for $d \approx 1.8$ m, is limited by the diameter of the FTL, see Fig. 3). We have simulated the beam that, after reflection on the SUT, is reflected by an imperfect 5P, then crosses the OI, the PBS, the FTL, and after two consecutive reflections on the FMs, it gets eventually focused on the CCD. We have modeled the surface defects of the optical components as single harmonics, with amplitude determined by the specification of the components in use (standard lab equipment). We have then adjusted the period and the phase of the each harmonic component, until a profile (Fig. 10, solid line) qualitatively similar to the experimental error signal (Fig. 9) was obtained. Doing this, we have re-scaled the amplitudes proportionally to the periods, a reasonable assumption for polished surfaces. The qualitative agreement between the simulation and the measurement confirms that the current surface quality of the elements in use is insufficient to endow the LTP sensitivity with an appropriate accuracy level.

If we now repeat the same exercise adopting tighter specifications for the optical tolerances (either $\lambda/40$ or even $\lambda/100$ – excluding the OIs, which already have a $\lambda/100$), we get the dashed lines in Fig. 10, which clearly describe a much more accurate scan of the angular range. The error signal now has a smaller amplitude – approx. 2 μrad and 1 μrad respectively – and much closer to the instrument sensitivity (0.2 μrad, see Sect. 2.2). When integrated over, e.g., a 500 mm-long mirror with a 2 km tangential curvature radius, this would be equivalent to a 1 nm peak-to-valley height error.

5. CONCLUSIONS AND FUTURE PLAN

We have described the LTP that has been built at LCLS for accurate metrology of mirrors, including bendable, highly-curved, and aspherical mirrors. We have shown a calibration of the instrument and a characterization of the measurement errors. The performances are currently limited by the optical quality of refractive and reflective parts, which have currently a figure specification of $\lambda/4 \div \lambda/20$, while it should be $\lambda/40$ or better. The replacement of these parts is in progress. Another improvement will result from the oncoming installation of the LTP in the new clean rooms at LCLS, on a solid basement and in a thermally isolated enclosure.

ACKNOWLEDGMENTS

This work is supported by US Department of Energy Office of Science. We thank Bianca Salmaso (INAF/OAB) for kindly providing us the thin glass samples we used to realize the phase plate.

REFERENCES

[1] Cocco, D., Abela, R., Amann, J.W., Chow, K.P., Emma, P.J., Feng, Y., Gassner, G.L., Hastings, J.B., Heimann, P.A., Huang, Z., Kelez, N.M., Loos, H., Montanez, P.A., Morton, D.S., Nuhn, H.D., Ratner, D.F., Rodes, L.N., Flechsig, U., Welch, J.J. and Wu, J., "The optical design of the soft x-ray self seeding at LCLS," Proc. SPIE 8849, 88490A (2013)

[2] https://lcls.slac.stanford.edu/instruments/l2si

[3] Von Bieren, K., "Pencil Beam interferometer for aspheric optical surfaces," Proc. SPIE 343, 101 (1982)

[4] Takacs, P.Z., Qian, S. and Colbert, J., "Design Of A Long Trace Surface Profiler," Proc. SPIE 749 (1987)

[5] Kilaru, K., Merthe, D,.J., Ali, Z., Gubarev, M., Kester, T., Benson, C., Mckinney, W., Tacacs, P. and Yashchuk, V., "Development of multi-beam long trace profiler," Proc. SPIE 8147, 814719 (2011)

[6] Qian, S., Jark, W. and Takacs, P.Z., The penta-prism LTP: A long-trace-profiler with stationary optical head and moving penta-prism, Review of Scientific Instruments 66(3), 25622569 (1995)

[7] Siewert, F., Noll, T., Schlegel, T., Zeschke, T., Lammert, H., "The nanometer optical component measuring machine: a new sub-nm topography measuring device for X-ray optics at BESSY," AIP Conf. Proc. 705, 847-850 (2004)

[8] Alcock, S., Sawhney, K., Scott, S., Pedersen, U., Walton, R., Siewert, F., Zeschke, T., Senf, F., Noll, T. and Lammert, H., The Diamond-NOM: A non-contact profiler capable of characterizing optical figure error with sub-nanometre repeatability, Nucl. Instrum. Meth. A, 616, 224228 (2010)

[9] Floriot, J., Levecq, X., Bucourt, S., Thomasset, M., Polack, F., Idir, M., Mercère, P., Brochet, S., Moreno, T., "Surface metrology with a stitching Shack-Hartmann profilometric head," Proc. SPIE 6616, 66162A (2007)

[10] Floriot, J., Levecq, X., Bucourt, S., Thomasset, M., Polack, F., Idir, M., Mercère, P., Moreno, T., Brochet, S., "A Shack-Hartmann measuring head for the two-dimensional characterization of X-ray mirrors," J. Synchr. Rad. 15, 134-139 (2008)

[11] Kirkpatrick, P. and Baez, A.V., "Formation of Optical Images by X-Rays," Journal of the OSA 38(9), 766 (1948)

[12] Cocco, D., Idir, M., Morton, D., Raimondi, L. and Zangrando, M., "Advances in X-ray optics: From metrology characterization to wavefront sensing-based optimization of active optics," NIM-A 907, 105-115 (2018)

[13] Nicolas, J., "Design of the LTP deflectometer," SLAC technical report (2017)

[14] Qian, S. and Takacs, P., "Equal optical path beam splitters by use of amplitude-splitting and wavefront-splitting methods for pencil beam interferometer," Proc. SPIE 5193 (2004)